UNIVERSIDAD NACIONAL AUTÓNOMA DE MEXICO
Posgrado en Astrofisica
Instituto de Astronomia

Towards a post MONDian formalism using clusters of galaxies.

TESIS QUE PARA OPTAR POR EL GRADO DE: MAESTRA EN CIENCIAS EN ASTROFISICA

PRESENTA: Shannon Rosslyn Escoto Navarro

TUTOR PRINCIPAL: Dr. Sergio Mendoza
[Instituto de Astronomia, UNAM]

COMITE TUTOR: Dra. Miriam Peña
[Instituto de Astronomia, UNAM]
Dra. Erika Benitez
[Instituto de Astronomia, UNAM]

Ciudad Universitaria, CD. MX., 12 DE JULIO DEL 2023

Towards a Post-MONDian formalism using clusters of galaxies.

Shannon Rosslyn Escoto Navarro

July 12, 2023

Contents

List of Figures

List of Tables

Acknowledgements

I would like to thank Dr. Gonzalo Olmo Alba, Dra. MariaFelicia de Laurentis, Dr. Xavier Nicolás Hernández Döring, Dra. Tula Bernal Marín and Dr. Tonatiuh Matos Chassin for reviewing this thesis.

It is my privledge to thank Universidad Autonoma de Mexico (UNAM) and the Astronomy Institute (IA) for all the support and knowledge they have given me. I thank support from a CONACyT scholarship (CVU 892812) and a DGAPA PAPIIT project (IN110522) I received during my Master's studies.

I would also like to thank my mom Ruth Escoto for her support throughout my master's and thesis journey as nothing would have been achieved without her encouragement and sacrifice.

I would like to thank my cousin Paola and my aunt Lorena for being there beside me throughout my studies and for always being supportive when I needed it.

Abstract

In this thesis the importance of the Mass-to-light ratio and the dynamical mass in calculating the theoretical mass and fitting it to observational data within the MOND limit to a fourth order perturbation is presented. It discusses the study of dark matter in galaxy clusters through X-rays, gravitational lensing, and rotation curves. It then moves on to discuss the history of our understanding of gravity, from Descartes' notion of occult fluids to Einstein's theory of general relativity. The use of the metric tensor and the principle of least action to calculate the geodesic trajectory of a test particle in a curved spacetime is used, as well as the use of clusters of galaxies to calibrate a relativistic modified Newtonian dynamics (MOND) model. The importance of clusters of galaxies in this calibration method is highlited and describes how the missing component in the cluster mass distribution can be determined by analyzing the temperature and gas profiles. Finally, a sample of clusters is used to calculate the theoretical mass and it shows how the baryonic mass needed can be calculated from observations by analyzing the baryonic density of gas in each cluster.

Chapter 1

Resumen

El uso de la relación masa-luz y la luminosidad total se utilizaron para inferir la masa de las galaxias. La relación masa-luz está relacionada con la edad de las poblaciones de estrellas dentro de una galaxia y su luz visible, y la relación aumenta a medida que la curva de rotación se aplana, proporcionando evidencia de materia oscura. El concepto de masa dinámica y masa total de un sistema es presentado. El estudio de la materia oscura en los cúmulos de galaxias se puede realizar a través de rayos X, lentes gravitacionales y curvas de rotación. El método más antiguo, que utiliza curvas de rotación, implica analizar la masa de los cúmulos observando la velocidad de los objetos en diferentes radios.

Se discute brevemente la evolución de la comprensión de la gravedad en la historia de la ciencia, que comienza con la noción de fluidos ocultos de Descartes en el siglo XVII, que asumía que el espacio no estaba vacío y tenía que contener algún tipo de fluido para explicar el movimiento planetario. Luego pasa a las leyes del movimiento planetario de Kepler y su tercera ley, que establece que el período de la órbita de un planeta al cuadrado es proporcional al cubo de su distancia al sol. Newton se basó en las leyes de Kepler para desarrollar sus propias leyes de movimiento y su ley de gravedad, que establece que la fuerza de gravedad entre dos objetos es proporcional al producto de sus masas e inversamente proporcional al cuadrado de la distancia entre ellos. El descubrimiento de Neptuno por LeVerrier y Adams en el siglo XIX debido a anomalías en la órbita de Urano condujo a un mayor refinamiento de nuestra comprensión de la gravedad. Finalmente, se analiza la teoría general de la relatividad de Einstein a principios del siglo XX, que reemplazó las leyes de Newton con una nueva teoría que describe la gravedad como la curvatura del espacio-tiempo causada por la presencia de masa y energía.

En el tercer capítulo se introduce el principio de equivalencia y el uso del tensor métrico para calcular la trayectoria geodésica de una partícula de prueba en un espacio-tiempo curvo. El principio de acción mínima se usa para determinar las variaciones nulas de la acción funcional que determina el movimiento de la partícula de prueba. La acción es un escalar, una cantidad invariante que se expresa como un funcional del tensor métrico $g_{\alpha\beta}$. Se define el Lagrangiano de una partícula libre y se utiliza una expansión de Taylor para reescribirlo con el fin de obtener correcciones relativistas. En el límite de aproximación del campo débil, el potencial escalar gravitacional ϕ se suma al Lagrangiano para tener en cuenta los efectos gravitatorios. Se introduce un espacio esféricamente simétrico e isotrópico y se obtiene una

métrica de espacio-tiempo simplificada implementando el radio de Schwarzschild. Finalmente, se introduce una constante de escala para asegurar que ambos términos en la ecuación métrica tengan las mismas dimensiones.

En el cuarto capítulo se describe el uso de cúmulos de galaxias para calibrar un modelo de dinámica newtoniana modificada relativista (MOND). Destaca la importancia de los cúmulos de galaxias como método de calibración debido a su simetría, estructura y tamaño, lo que facilita su análisis. Los cúmulos de galaxias tienen un medio intracúmulo (ICM) compuesto principalmente por hidrógeno ionizado y helio, que emite radiación principalmente en el espectro de rayos X. Con esto, el componente que falta en la distribución de masa del grupo se puede determinar mediante el análisis de los perfiles de temperatura y gas. Se describe la aceleración del radio del cúmulo en relación con la temperatura y el potencial gravitacional para un sistema en equilibrio gravitatorio. Finalmente, se muestra que las partículas de masa de los cúmulos de galaxias se pueden explicar usando solo su masa bariónica y los resultados del cuarto orden de perturbación de MOND del capítulo anterior.

Chapter 2

Introduction

The use of mass-to-light ratio and total luminosity were used to infer the mass of galaxies. Mass-to-light ratio is related to the age of star populations within a galaxy and its visible light, and the ratio increases as the rotation curve flattens, providing evidence for dark matter.The concept of dynamical mass and total mass of a system is presented. The study of dark matter in galaxy clusters can be done through X-rays, gravitational lensing, and rotation curves. The oldest method, using rotation curves, involves analyzing the mass of clusters by observing the velocity of objects at different radii.

§2.1 Mass to light ratio and total L to infer mass

The colors of galaxies provide much of the information there is about their age, elements and luminosity. The luminosity of a galaxy is an extremely important aspect as it has been proven to be very useful when calculating the mass of galaxies using the ratio between them. This mass-to-light ratio Υ is refered to the values of the Sun in the Solar System* and is related to the age of the populations of stars within the galaxy and its visible light. This can be directly related to the H-R diagram where the lower main sequence stars evolve as the mass-to-light ratio increases.

Mass-to-light ratios gained a lot of popularity with the development of rotation curves of spiral galaxies in the 1960's and 1970's. These rotation curves were showing a steep rise at the inner parts of a galaxy, reaching a maximum, continuing with a brief descending Keplerian pattern and then reaching quite flat profiles on the external parts. This was fully demonstrated by Burbidge et al. (1961), with the observations of the full rotation curve and mass of the galaxy NGC157, where further distance measurements were impossible at that time due to the low brightness at a larger radius. It was broadly assumed that the rotation curve would follow a Keplerian fall, but it was not until HI spectral line observations at 21 cm wavelength showed that these rotation curves did not descend but rather, flattened.

Under the assumption of a spherical mass distribution for galaxies, the local mass-to-light ratio would increase as the rotation curve flattens and so, this comparison gave this ratio its major role since at first sight this provides evidence for an "undetected" mass, or dark matter.

*The mass-to-light ratio of the sun $\Upsilon_\odot = 5133\text{kg/W}$. As mentioned in the text, in astronomy units are chosen such that $\gamma_\odot = 1$.

For pressure supported systems, such as galaxy clusters, the mass-to-light ratio M/L changes very rapidly towards the central part of the systems, i.e. when the radial distance $r \to 0$ as shown by the early observations of the Virgo Cluster by Smith (1936).

§2.2 Dynamical mass

Under the assumption of spherical symmetry, the mass $M(r)$ contained within a sphere of radius r is given by:

$$M(r) = 4\pi \int_0^r r'^2 \rho(r')\, \mathrm{d}r' \,. \tag{2.1}$$

For a circular orbit, Kepler's third law implies that the centripetal acceleration a, is given by:

$$a = \frac{v^2}{r}, \tag{2.2}$$

where v represents the orbital velocity of a test particle at radius r. In gravitational equilibrium, the centripetal acceleration is balanced with the gravitational one and so:

$$M_{\mathrm{dyn}}(r) = -\frac{v^2 r}{G}, \tag{2.3}$$

where G is Newton's gravitational constant and $M_{\mathrm{dyn}}(r)$ represents the *dynamical mass* within r of the system under study.

The total mass M_{T} of the system is given by the sum of the gas M_{gas}, the mass of stars M_{stars} and the dark matter component M_{DM} (cf. §2.4):

$$M_{\mathrm{T}} = M_{\mathrm{gas}}(r) + M_{\mathrm{stars}}(r) + M_{\mathrm{DM}}(r). \tag{2.4}$$

§2.3 Dark matter in clusters of galaxies

Zwicky (1933) tried to find an explanation of the problems with the inferred mass and the big dispersion of velocities in dense clusters of galaxies. He analyzed the dispersion of velocities in the Coma cluster, with differences of about 1500 – 2000 km/s. He was able to deduce that in order to account for such difference, the average density of the Coma cluster would have to be 400 times greater than the luminous matter seen in the observations if the system was to be considered stationary (Zwicky, 1933).

Given that current observations of spiral galaxies do not present a Keplerian fall on their rotation curve, and since the rotational velocity is proportional to the 1/4th power of their mass, the solution to this discrepancy and the relationship between the M/L ratios was to add some sort of "missing" mass or "dark matter".

Galaxy clusters are quite important when it comes to the study of dark matter because their mass can be calculated in several ways:

- **X-rays**: Clusters have a large amount of galaxies with $\sim 10^{10}$ stars within each of them. This allows astronomers to see the hot gas in between each of these galaxies as X-rays

cooling flows (Fabian et al., 1987). The X-ray observations yield density, pressure and mass profiles (e.g. Paterno-Mahler et al., 2017).

- **Gravitational lensing**: When a ray of light approaches a massive object, a bending on the ray's trayectory occurs. This phenomenon allows the mass distribution of clusters to be determined. Weak gravitational lensing is specially important as it allows numerical simulations to be linked with the information from baryonic mass tracers (e.g. Hoekstra et al., 2013).

- **Rotation curve**: Finally, the oldest method and the one discussed in Section §2.1 consists on the determination of the mass of clusters of galaxies by analyzing the rotational velocities, through their mass profiles, using their mass-to-light ratio M/L.

The infered mass between various methods yield a very accurate determination of the missing dark matter in different astrophysical scenarios.

§2.4 Dark matter in spiral galaxies

Spiral galaxies are a "special" type of galaxies as they are the most symmetrical ones, since everything in them, and mainly within the disk, is moving on a nearly circular orbit about its center, and are in rotational equilibrium acording to equations (2.2) and (2.3). Due to their symmetry, the mass of spherical galaxies give a good and direct approximation when it comes to their rotation curve.

As already mentioned in Section §2.1, the rotation curve is a direct approximation of the velocity following Kepler's 3rd law ($v^2 \propto M/r$). When measuring the galaxy's mass (M) using the 21-cm H line, the flattening of the resulting curve can be mostly completely accounted for with the "missing" matter. Hence, a dark halo model was developed by using this missing or "dark" matter and distributing it throughout the galaxy's model, so that, the contribution to the total rotation curve is given by the disk, the stars, gas and dark matter halo (Salucci & Persic, 1997).

§2.5 Dark matter in spiral galaxies: the Tully-Fisher relation

The dark matter halo model mentioned in the previous section has a catch: it does not follow Kepler's 3rd law. The relation between the rotational velocity v and the baryonic mass of the system is given by:

$$v^4 \propto M, \tag{2.5}$$

and is commonly called the Tully-Fisher relation (see Section §3.5):

The relationship between the amount of mass and the velocity can be interpreted in such a way that there most be some type of undetected dark matter around the spiral galaxy in order to keep the velocity at a constant rate such that the rotation curves flattens at sufficiently large distances away from the center.

§2.6 Dark matter in cosmology

When thinking about physics and the universe, it is common to apply Einstein's theory of General Relativity (GR). The concordance ΛCDM (Cold Dark Matter) cosmological model of the universe (Melia, 2022) uses GR field equations given by:

$$G_{\mu\nu} + \Lambda g_{\mu\nu} = \kappa T_{\mu\nu}, \tag{2.6}$$

$$G_{\mu\nu} = R_{\mu\nu} - \frac{1}{2} g_{\mu\nu} R = 8\pi G T_{\mu\nu}, \tag{2.7}$$

where R is Ricci's scalar, $T_{\mu\nu}$ the stress energy tensor, $g_{\mu\nu}$ the metric tensor and Λ the cosmological constant.

An homogeneous and isotropic universe is described by the Friedmann, Lemaître, Robertson and Walker (FLRW) metric given by:

$$\mathrm{d}s^2 = \mathrm{d}t^2 - a^2(t)\,\mathrm{d}l^2\,, \tag{2.8}$$

where $\mathrm{d}l^2$ describes the geometry of space with respect to a value κ that describes the curvature of the 3-space and $a(t)$ is a dimensionless scale factor, normalized to a present day value of $a_0 = 1$.

The curvature of space κ yields three different dynamical models when no dark matter nor dark energy are introduced: (a) an open universe if $\kappa = -1$, (b) a flat universe if $\kappa = 0$ and (c) a closed universe if $\kappa = 1$. The first two cases correspond to expanding models and the third is a re-collapsing one. The concordance model corresponds to a measured value $\kappa = 0$. The rate of expansion of the universe at the present epoch $H(t_0) := \dot{a}(t_0)$ is the first cosmographical parameter (Capozziello & De Laurentis, 2011) with a value of ~ 70km/sMpc.

The Cosmic Microwave Background Radiation (CMBR) has been one of the most important tools used in Cosmology since its discovery, being the oldest light in the universe, it provides important information about the early universe. Its temperature is not the same all throughout space and fluctuates slightly from place to place. These small fluctuations are referred to as the temperature anisotropy of the CMBR and are the footprints of density fluctuations that eventually collapsed to form the structure of our universe (Tkachev, 2018). Observations showed temperature fluctuations of the order of 10^{-5} and did not match the expected measurements of a fully baryonic matter universe (which correspond to values of the order of 10^{-3}) as these fluctuations would not have been able to evolve into the structure of the universe we observe at the present epoch. Using a prominently dark matter universe allows for the complete formation and evolution of these structures which are consistent with the observations. These theoretical models use non-relativistic or "cold" non baryonic dark matter particles and represent the basis for the concordance cosmological model.

The ΛCDM cosmological model introduces a cosmological constant Λ term on the field equations of general relativity that introduce an accelerated expansion, since observations of SNIa and CMBR require such term in order to be explained (Puget, 2021; Durrer, 2020).

Dark energy was theorized from the fact that a matter dominated universe did not predict the correct Hubble constant, and neither predict the age of the universe. But it was not

until Supernova observations (Perlmutter et al., 2003) and their nearly uniform luminosities, which in turn, showed that the universe was not decelerating, but in fact it was accelerating. The simplest idea was to assumme that a scalar energy field, the cosmological constant, was responsable of this expansion.

Chapter 3

Extending gravity

The evolution of the understanding of gravity in the history of science is briefly discussed, it starts with Descartes' notion of occult fluids in the 17th century, which assumed that space was not empty and had to contain some sort of fluid to explain planetary motion. It then moves on to Kepler's laws of planetary motion and his third law, which states that the period of a planet's orbit squared is proportional to the cube of its distance from the sun. Newton built on Kepler's laws to develop his own laws of motion and his law of gravity, which states that the force of gravity between two objects is proportional to the product of their masses and inversely proportional to the square of the distance between them. The discovery of Neptune by LeVerrier and Adams in the 19th century due to anomalies in Uranus' orbit led to the further refinement of our understanding of gravity. Finally, the chapter discusses Einstein's theory of general relativity in the early 20th century, which replaced Newton's laws with a new theory that describes gravity as the curvature of spacetime caused by the presence of mass and energy.

§3.1 Descartes and occult fluids

In 1644, Philosopher and Mathematician Rene Descartes started introducing the notion of *occult fluids* in his published manuscript *Principles of Philosophy* (see e.g. Miller, 1984). In this manuscript he explained that the existence of empty space is impossible and he assumes space as being similar to a body, i.e. empty space has to contain something and not be "empty". Given this statement, the Universe most be filled with some sort of fluid. In other words, vacuum is described as an undetected matter flow, moving through space. He was able to explain the motion of the planets about the sun, using the idea that the planets rotate because of vorticity produced by this occult fluid. The moons of the different planets rotate about them since other vortices attached to the planets produce circular motions of these satellites (Spratt, 2016).

§3.2 Newton's Principia, Kepler 3rd law and the theory of gravity

In the 1620s, Johannes Keppler published the book *Harmonices Mundi Libri IV*. This book was very important at the time as he acknowledges the Sun as the source of movement for the planets. Here, taking the driving force of the Sun as $1/r$ and using the patterns in the amount and volume of the matter seen in his *Messekunst Archimedis (1616)*, the volume is then taken as a function of r.

Using the planetary data in his *Messekunst Archimedis (1616)* he approximates that the ratio between the amount of matter in a planet and it volume (density) was proportional to $1/\sqrt{r}$ The amount of matter can also be described as being proportional to $\sqrt{r}$ and he introduces the first idea:

$$\text{Period} = \frac{\text{Length of path}}{\text{strength of driving force}} \times \text{density} = \frac{r}{1/r} \times \frac{1}{\sqrt{r}}, \tag{3.1}$$

so that,

$$P \propto \text{Period} \times \text{density} = \frac{r}{1/r}\frac{\sqrt{r}}{r} = r^{3/2}, \tag{3.2}$$

where the distance of a planet from the Sun had to be proportional to the size of the planet, its surface or its volume.

Therefore, his now known 3rd law of planetary motion is given by:

$$T^2 \propto a^3, \tag{3.3}$$

where T is the period and a the length of the semi-major axis distance of the orbit (Gingerich, 1975).

According to Kepler's 1st law of planetary motion, test particles or planets follow an elliptical orbit. For many astronomical purposes (the planets on the solar system), the assumption of a circular orbit is coherent and so, using Kepler's 2nd law of planetary motion (test particles sweep equal areas in equal times), the velocity of a test particle is $v = \text{const}$ and so, the period $T \propto 2\pi r/v$. In other words:

$$v \propto \sqrt{\frac{M}{r}}. \tag{3.4}$$

It was Isaac Newton, who took advantage of the previous information in his *Philosophia Naturalis Principia Mathematica* (1687). He Assumed that gravity was a force and to put things simple for the purpose of this work, under the assumption of a circular motion of a planet about the Sun, the centripetal acceleration $a = v/r$ and so, using Kepler's third law (3.3) it then follows that:

$$a = \frac{v^2}{r} = -G\frac{M}{r^2}, \tag{3.5}$$

where Newton's constant of Gravity G is a proportionality constant that is calibrated with the motion of planets and the minus sign represents the attractive force of gravity. As a side note, Newton actually found Descartes' idea of a fluid problematic, since its existence would

not allow planets to move freely through space due to the fluid's resistance (Spratt, 2016).

§3.3 LeVerrier, Adams and Neptune. LeVerrier and Vulcan

Alexis Bouvard (1821) showed with his *Tables astronomiques* (see e.g. Jarrell, 2007) that the motion of Uranus (discovered in 1781) was irregular since it sometimes fell behind and some others appear forward from the predictions of Newton's theory of gravity. He hypothesized that this discrepancy of the planet's orbit could be due to (a) its great distance to the Sun, where Newton's gravitation theory could fail, (b) by some perturbation felt by Uranus from another body (maybe an 8th planet) or (c) by observational errors.

Independently, in 1845, Urbain LeVerrier and Adams predicted that the anomaly in Uranus' orbit had to be due to the presence of an undetected planet beyond it. LeVerrier gave these calculations and predictions to the Astronomer Joham Galle in Berlin and this was when and how Neptune was able to be observed. Independenly, Mathematician John Adams had already started looking into the motion of Uranus as early as 1841. It was also in 1845 that he gave James Challis, in Cambridge, the calculation to the location of this new planet beyond Uranus. Unfortunately, it was not until LeVerrier's discovery in Berlin, that Adam's calculations of Neptune were able to be recognized. This is how they both came to be known as the discoverers of Neptune (see Smart, 1947, for more information).

Later on, in 1855, LeVerrier, also intrigued by the precession in Mercury's orbit, which was also not explained with Newton's theory, hypothesized that either a small planet or a cluster of small planets had to be inside Mercury's orbit in order to account for its residue value*. In 1859, amateur Astronomer Lescarbault watched a small black dot crossing the Solar disc –which resembled the transit of a planet about the Solar disc. He sent LeVerrier his findings, whom he met later and concluded that he had detected the 9th planet of the Solar System (Fontenrose, 1973).

This planet was given the name Vulcan and up to now has never been found. It wasn until 1914 when Einstein was able to explain Mercury's movement with his theory of General Relativity.

§3.4 Extending Newtonian gravity towards a relativistic regime: General Relativity

Albert Einstein completed his theory of Special relativity in 1905, but it was not until 1915, that he completed his, now famous, theory of General Relativity (GR). As mentioned in section §2.6 Einstein's field equations were able to perfectly match the observations of the precession in Mercury's orbit. This discovery did not cancel out Newton's gravity but only limited its applications. For example, in the weak field limit of GR, equation (2.7) can be reduced to Newton's equations.

*All planets in the solar system show precession of their perihelium about the Sun. When the influence of all planets on a particular one are taken away (so that the planet's motion interacts only with the Sun's gravitational force) then, this perihelium precession vanishes, except for Mercury. This is why Le Verrier's hypothesis of a possible inner planet(s) beyond Mercury's orbit is coherent.

Einstein's theory of gravitation takes space and time to be within the same structure called "*space-time*" with a local inertial reference frame containing local flat coordinates which follow the straightest paths in curved spaces called geodesics (Capozziello & De Laurentis, 2011).

The symmetric Energy-momentum tensor $T_{\mu\nu}$ shown in equation (2.7) is of extreme importance as it gives information about the matter and pressure content (energy and momentum) across all space-time (see e.g. Landau & Lifshitz (1976); Mendoza & Silva (2021)).

The line element $\mathrm{d}s$ in space-time is given by:

$$\mathrm{d}s^2 = g_{\mu\nu}\,\mathrm{d}x^\mu\,\mathrm{d}x^\nu\,, \tag{3.6}$$

where $g_{\mu\nu}$ is the metric tensor and in what follows we assumme a metric signature $(+,-,-,-)$

For the case of an empty flat Minkowski space-time, the interval in Cartesian (ct,x,y,z) and spherical coordinates (ct,r,θ,ϕ) is given by:

$$\mathrm{d}s^2 = c^2\,\mathrm{d}t^2 - \mathrm{d}l^2 = c^2\,\mathrm{d}t^2 - \mathrm{d}r^2 - r^2\,\mathrm{d}\theta^2 - r^2\sin^2\theta\,\mathrm{d}\phi^2\,, \tag{3.7}$$

where $\mathrm{d}l := \sqrt{\mathrm{d}x^2+\mathrm{d}y^2+\mathrm{d}z^2}$ is the Cartesian space-line element.

In order to use the field equations and compare them to astrophysical observations, corrections have to be made to the metric. These corrections or perturbations are very small. Taking the fact that the metric tensor $g_{\mu\nu}$ is the same as the Minkowski metric $\eta_{\mu\nu}$ in the weak field limit of approximation, the correction $h_{\mu\nu}$ is made for $|h_{\mu\nu}| \ll |\eta_{\mu\nu}|$. These perturbations are estimated to an $\mathcal{O}(4)$ in a later section. Here and in what follows $\mathcal{O}(n)$ refers to $\mathcal{O}(1/c^n)$. Therefore, when looking for the metric components at perturbation order $\mathcal{O}(0)$, $\mathcal{O}(2)$, $\mathcal{O}(4)$ and $\mathcal{O}(6)$ it means corrections at $\mathcal{O}\big(1/c^0\big)$, $\mathcal{O}\big(1/c^2\big)$, $\mathcal{O}\big(1/c^4\big)$ and $\mathcal{O}\big(1/c^6\big)$ (for more information about this, see Bernal et al., 2019a, and Section §4.5).

§3.5 Tully-Fisher law and path to MOND

As mentioned in section §2.5 the external parts of, galaxy rotation curves do not follow Kepler's law, Tully & Fisher (1977) derived the distance to the Virgo and Ursa Major clusters using HI (21-cm) line observations and the known distances to two nearby groups: M81 and M101 as comparison. They were able to find a relationship between the spiral galaxy's magnitude and its rotational velocity to calculate the distance to them with their luminosity being dependent on the wavelength band that was being measured from. The relationship fitted the known information of spiral galaxies well (Tully & Fisher, 1977).

This relation was used for many decades, but McGaugh et al. (2000) rewrote that relationship in terms of the rotational velocity of stars and the baryoinic mass of disk galaxies, finding:

$$M \propto v^4. \tag{3.8}$$

Under the assumption that gravity deviates from its Newtonian expression at those Tully Fisher scales observed in spiral galaxies, where rotation curves flatten, it can be stated that the Tully Fisher relation is a replacement to Kepler's third law. In other words, the Tully

Fisher expression is an extended Kepler's third law at sufficiently large scales. At small scales such as the one associated to the solar system, or the central parts of a spiral galaxy, Keper's third law holds. Under these assumptions, the Tully-Fisher law for a circular orbit, where the centripetal acceleration $a = v^2/r$ yields (Mendoza, 2015b):

$$a = -G_M \frac{M^{1/2}}{r} \tag{3.9}$$

where the modified gravitational constant $G_M = 8.94 \times 10^{-11}\,\mathrm{m^2\,s^{-2}\,kg^{-1/2}}$ is calibrated using rotation curves of spiral galaxies.

Milgrom (1983) considered a very simple form of modification to Newton's 2nd law, by allowing a proportionality between inertia and acceleration with the use of an interpolation function $\mu(x)$:

$$F = \mu\left(\frac{a}{a_0}\right) ma, \qquad \mu = \begin{cases} 1, & |x| \gg 1 \quad \text{(Newton's limit)}, \\ x, & |x| \ll 1 \quad \text{(Tully-fisher limit)}, \end{cases} \tag{3.10}$$

where $x := a/a_0$ and m is the mass of a particular test particle. He introduced the acceleration constant a_0 as a turning point between the two limits. For accelerations much greater than a_0, Newton's dynamics and Kepler's third law hold. However, for accelerations much smaller than a_0, T-F dynamics are obtained.

The transition acceleration a_0, or Milgrom's acceleration constant, was able to be deduced by Mendoza & Olmo (2015) by comparing equations (3.5) and (3.9), yielding:

$$a_0 = \frac{G_M^2}{G_N}. \tag{3.11}$$

Therefore, the acceleration of a rotating system in terms of a_0 allowed for a deep MOdified Newtonian Dynamics (MOND) regime, i.e. $a << a_0$:

$$a = \frac{(a_0 G M)^{1/2}}{r}, \tag{3.12}$$

with the Tully-Fisher law given by:

$$v = G_M^{1/2} M^{1/4}. \tag{3.13}$$

§3.6 AQUAL

Unfortunately, MOND is not a physical theory. Milgrom tried to use observational data to confirm this theory but found issues when e.g., momentum was not conserved when applied to N-body systems and when calculating the center of mass of a star, since the acceleration would follow MOND but the galaxy where the star is in would follow Newtonian dynamics. He could not find an explanation as to why these two would be different if one comes from the other. Additionally, MOND is not able to explain the gravitational lensing explained by GR since it is a non-relativistic proposal (Milgrom, 1983).

Bekenstein & Milgrom (1984) tried tackling these issues using the gravitational Poisson equation and its properties for massive objects and their density ρ:

$$\nabla^2\varphi = 4\pi G\rho, \tag{3.14}$$

where φ is the Newtonian gravitational potential. Equation (3.14) is obtained by the null variations of the field ϕ of the following Newtonian gravitational action (Mendoza, 2015a):

$$\mathcal{S}_{\rm N} = -\int \mathrm{d}^3x \left[\frac{1}{8\pi G}\left(\nabla\varphi\right)^2 + \rho\varphi\right] = \int \mathrm{d}^3x\, \mathcal{L}_{\rm N}(\varphi, \varphi_{,k}\,; x_k), \tag{3.15}$$

The modification at the action level appeared through the introduction of an AQUAdratic Lagrangian (AQUAL) $\mathcal{L}$ where the gravitational Lagrangian density $\mathcal{L}_{\rm N}$ is a function of the field φ and its derivatives $\varphi_{,k}$ with respect to the spatial coordinates x_k. In order to make a small modification to it and still have a potential φ from which the acceleration can be derived, they used $F(x^2)$ as an arbitrary function of itself with a_0 as a scaling constant for the acceleration needed for any non-Newtonian case:

$$\mathcal{L}_{\rm AQUAL} = -\frac{a_0^2}{8\pi G}\ F\left(\frac{|\nabla\varphi|^2}{a_0^2}\right) - \rho\Phi. \tag{3.16}$$

This was the first non-relativistic approach to MOND for small accelerations with the condition that $|\nabla\varphi| \to 0$ as the radius $r \to \infty$ so that the acceleration $\boldsymbol{a}$ of a test particle can be given by

$$|\boldsymbol{a}| = |\nabla\varphi|. \tag{3.17}$$

A relativistic AQUAL (RAQUAL) was then approached but it encountered that at small perturbations, the gravitational waves would start propagating at superluminal speeds, creating a gravitational potential that not only does not explain the light deflection previously explained with GR, but showing that the potential is affecting the bending of the light as well (Bekenstein & Milgrom, 1984; Bekenstein, 2005).

§3.6.1 TeVeS (Tensor-Vector-Scalar)

With the intention of building a relativistic theory of MOND, Bekenstein (2005) introduced TeVeS building an extended gravitational action (see Section §4.1) to keep all of the conservation laws intact. This construction uses the standard metric *Te*nsor a timelike *Ve*ctor field u_μ, a dynamical scalar field ϕ, a non dynamical *S*calar field σ (*TeVeS*) for the gravitational Lagrangian. This proposal was able to explain gravitational lensing at low accelerations. Although TeVes was proven useful, it was also proven to be inconsistent when it comes to systems under hydrostatic equilibrium such as stars, since they became very unstable. It is also inconsistent with cosmic microwave background radiation acoustic peaks, lensing in the bullet cluster and LIGO's measurement of gravitational waves (Lars et al., 2019).

§3.7 Non-relativistic extended gravity. Mendoza et al. (2011)

Mendoza et al. (2011) generalized equation (3.12) using dimensional analysis and concluding that a general statement can be made about the acceleration force for gravitational systems:

$$\frac{a}{a_0} = f(x) \to \begin{cases} x^2, & \text{for Newton's gravitational acceleration,} \\ x, & \text{for MOND's acceleration,} \end{cases} \tag{3.18}$$

where $x := l_M/r$ and $l_M := (GM/a_0)^{1/2}$. By taking these two acceleration limits of $f(x)$ and expanding them as geometric series, they were able to propose a transition function from the MONDian limit to the Newtonian one:

$$\left(\frac{a}{a_0}\right)_{\pm} = f(x) = x\frac{1 \pm x^{n+1}}{1 \pm x^n}. \tag{3.19}$$

The free parameter n was calibrated using the rotation curve of our galaxy (Famaey & Binney, 2005) and concluded that the best fit ocurred for $n \approx 3$ with negative signs used in (3.19).

Now, using Poisson's equation (3.14) and Green's theorem for very symmetric systems, one can rewrite the acceleration vector with its unit vector as follows:

$$\left(\frac{\boldsymbol{a}}{a_0}\right)\left(\frac{x^2}{f(x)}\right) = x^2\boldsymbol{e}_a = -\frac{G}{a_0}\int \frac{(\boldsymbol{r}-\boldsymbol{r'})}{|\boldsymbol{r}-\boldsymbol{r'}|^3}\rho(\boldsymbol{r'})\,\mathrm{d}V'\,. \tag{3.20}$$

Chapter 4

Post MONDian parametrization

The principle of equivalence and the use of the metric tensor for calculating the geodesic trajectory of a test particle in a curved spacetime is introduced in this chapter. The principle of least action is used to determine the null variations of the functional action that determines the motion of the test particle. The action is a scalar, an invariant quantity that is expressed as a functional of the metric tensor $g_{\alpha\beta}$. The Lagrangian of a free particle is defined and a Taylor expansion is used to rewrite it in order to obtain relativistic corrections. In the weak field limit of approximation, the gravitational scalar potential ϕ is added to the Lagrangian to account for gravitational effects. A spherically symmetric and isotropic space is introduced and a simplified spacetime metric is obtained by implementing the Schwarzschild radius. Finally, a scaling constant is introduced to ensure that both terms in the metric equation have the same dimensions.

§4.1 Principle of equivalence

Mentioned for the first time by Newton (1729) in his Philosophiæ Naturalis Principia Mathematica, Newton's second law $F = ma$ combined with the gravitational law $F = mg$ impliedthat "mass is proportional to its weight".

It was Einstein who, centuries later, proposed the example of an observer inside a free falling elevator and explained that the observer would see all bodies in its same gravitational field as falling at the same acceleration and thus feeling no acceleration at all. This complimented Newton's idea that the inertial and gravitational mass of bodies would be the same during free fall. This could in principle be extended to all laws of physics in what is referred to as the *Weak Equivalence Principle*(WEP).

Taking all of this into account Einstein made a postulate stating that as long as the WEP is valid, the outcome of any experiment would be independent from its place or time in the universe. Regardless of its composition, its structure or even its velocity. Counting on its inhomogeneities to be sufficiently small to be ignored in a free falling frame. This is what is now called the Einstein Equivalence Principle (EEP). Accordingly, one can assign a metric to the space-time, geodesics to the straight lines of that space-time manifold and a Lorentz Invariance to the physical laws following special relativity, which are the same for different observers (Will, 2018).

§4.2 Metric $\mathcal{O}(2)$ in g_{00} using the gravitational action for a free massive particle

The interval ds between two infinitesimal points in a curved space-time is given by:

$$\mathrm{d}s^2 = g_{\alpha\beta}\mathrm{d}x^\alpha \mathrm{d}x^\beta, \tag{4.1}$$

for a metric tensor $g_{\alpha\beta}$. In here and in what follows, Greek indices have values of 0,1,2,3 and Latin ones have values of 1,2,3. Also, an Einstein summation convention over repeated indices is used throughout the text.

The principle of least action yields the equations of motion of a test particle between two points in a system. The geodesic trajectory of such particle is described by requiring a functional action S to reach a minimum value. In practice it is the null variations $\delta S = 0$, i.e. the extremum of the functional S, that determines such motion. The action is a scalar and as such it is invariant (Mendoza, 2015a) given by (Landau, 2013):

$$S = -mc\int_a^b \mathrm{d}s = \int_a^b \left(g_{\alpha\beta}\mathrm{d}x^\alpha \mathrm{d}x^\beta\right)^{1/2} = \int_{t_1}^{t_2} L\mathrm{d}t, \tag{4.2}$$

where L is the Lagrangian of the system. For a free particle in a flat Minkowski space-time, the Lagrangian is given by $L = -mc^2\sqrt{1-v^2/c^2}$. The non-relativistic action is obtained in the limit where $c \to \infty$ and as such, in order to obtain relativistic corrections to this non-relativistic limit, a Taylor expansion is used to rewrite the Lagrangian as:

$$L = -mc^2\left[1 - \frac{1}{2}\frac{v^2}{c^2} - \frac{1}{8}\left(\frac{v^2}{c^2}\right)^2 - \frac{1}{16}\left(\frac{v^2}{c^2}\right)^3\right] + \mathcal{O}(4) \tag{4.3}$$

Substitution of equation (4.3) into (4.2) yields:

$$\mathrm{d}s = \left(c - \frac{v^2}{2c}\right)\mathrm{d}t\,,$$

and since $v\,\mathrm{d}t = \mathrm{d}r$ it turns out that:

$$\mathrm{d}s^2 = c^2\left(1 + \frac{v^4}{4c^4}\right)\mathrm{d}t^2 - \mathrm{d}r^2\,. \tag{4.4}$$

at $\mathcal{O}(4)$ of approximation.

Thus, for the case of a Minkowski space-time and comparing equation (4.4) with equation (3.7), the terms smaller than $\mathcal{O}(2)$ are neglected and so, the non-null metric tensor components are given by:

$$g_{00} = 1, \qquad \text{and} \qquad g_{11} = -1. \tag{4.5}$$

In the general case, when gravitational effects are taken into account, particles do not only move in a straight lines due to the curvature of space. To account for gravitational effects in the weak field limit of approximation, one can add the gravitational scalar potential ϕ to the Lagrangian L. In other words, for the case of a general curved space-time in the weak field

limit of approximation, the Lagrangian L at $\mathcal{O}(4)$ is given by:

$$L \approx -m\left[c^2 - \frac{v^2}{2} + \phi + \cdots\right], \tag{4.6}$$

and so:

$$\mathrm{d}s^2 = \left[c^2 - v^2 + 2\phi + \frac{1}{c^2}\left(\phi^2 - \phi v^2 + v^4\right)\right] dt^2 = (c^2 + 2\phi)\,\mathrm{d}t^2 - dr^2, \tag{4.7}$$

i.e. at $\mathcal{O}(2)$ of approximation is follows that:

$$g_{00} \;=\; 1 + \frac{2\phi}{c^2}. \tag{4.8}$$

§4.3 Schwarzschild space-time

A spherically symmetric and isotropic space is then introduced with the interval $\mathrm{d}s$ as a change in distance from a particular origin. Coordinates can then be described as $(x^0, x^1, x^2, x^3) = (ct, r, \theta, \phi)$, where r is the radial coordinate and θ and ϕ represent the polar and azimuthal angles, with an angular displacement defined as $\mathrm{d}\Omega^2 = \mathrm{d}\theta^2 + \sin^2\theta\,\mathrm{d}\phi^2$

Schwarzschild (Landau, 2013) implemented the constant of length named gravitational radius or Schwarzschild radius

$$r_g = \frac{2GM}{c^2}, \tag{4.9}$$

to yield a simplified spacetime metric adequate for a point mass source M, which in Schwarzschild coordinates, is relevant for an observer at rest at infinity, yields:

$$ds^2 = \left(1 - \frac{r_g}{r}\right) c^2\,\mathrm{d}t^2 - \left(1 - \frac{r_g}{r}\right)\mathrm{d}r^2 - r^2\,\mathrm{d}\Omega^2\,. \tag{4.10}$$

By means of Birkhoffs theorem. the external Schwarzschild solution can be extended to any sperical mass distribution $M(r)$ (Townsend, 1997).

§4.4 PPN parameters

The null variations of the action (4.2) yield the equation of motion for a test particle on a curved space-time:

$$\frac{\mathrm{d}^2x^\alpha}{\mathrm{d}s^2} + \Gamma^\alpha_{\beta\lambda}\frac{\mathrm{d}x^\beta}{\mathrm{d}s}\frac{\mathrm{d}x^\lambda}{\mathrm{d}s} = 0, \tag{4.11}$$

where the Christoffel symbols $\Gamma^\alpha_{\beta\eta}$ are given by:

$$\Gamma^\beta_{\lambda\mu} = \frac{1}{2}\left(\frac{\partial g_{\mu\beta}}{\partial x^\lambda} + \frac{\partial g_{\mu\lambda}}{\partial x^\beta} - \frac{\partial g_{\beta\lambda}}{\partial x^\mu}\right), \tag{4.12}$$

At $\mathcal{O}(4)$ of approximation, the Ricci scalar is given by:

$$R = \cancelto{0}{{}^{(0)}R} + {}^{(2)}R + {}^{(4)}R + \mathcal{O}(6). \tag{4.13}$$

Note that the first $\mathcal{O}(0)$ term on the right-hand side of the previous equation is zero in accordance with a flat space-time at the lowest perturbation order.

The traditional idea of building a relativistic theory of gravity is that its WFL of approximation is Newtonian gravity, i.e. the WFL of approximation should converge to Poisson's equation (3.14), as it can be seen from the results of Section §4.2 at perturbation order $\mathcal{O}(2)$. The terms to order $\mathcal{O}(4)$ or higher must be taken into account when dealing with relativistic corrections to the Newtonian limit. With this, a higher order Lagangian can be constructed (Will, 2018):

$$L = c^2\left(1 - \frac{2\phi}{c^2} - \frac{v^2}{c^2} - g_{00}[\mathcal{O}(4)] - 2g_{0j}[\mathcal{O}(3)]\frac{v^j}{c} - g_{jk}[\mathcal{O}(2)]\frac{v^j}{c}\frac{v^k}{c}\right)^{1/2}. \tag{4.14}$$

The first three terms represent the Lagrangian function of a free particle to order $\mathcal{O}(2)$ and the following terms are the post-Newtonian terms to order $\mathcal{O}(4)$.

In other words, the PPN approximation requires knowledge of the metric components in the following way:

$$\begin{aligned} g_{00} &\text{ up to } \mathcal{O}(4), \\ g_{0j} &\text{ up to } \mathcal{O}(3), \\ g_{jk} &\text{ up to } \mathcal{O}(2). \end{aligned} \tag{4.15}$$

Assuming that the system is a perfect fluid the restrictions to be taken into account when deriving the above terms are (Will, 2018):

- Metric components should be dimensionless quantities and should converge to their Minkowskian values at large distances since space-time is asymptotically flat.
- There is not a unique reference frame to be chosen. Initial conditions, i.e. initial points on the space-time manifold, can be arbitrary.
- Correction terms to the metric should transform with the same rules as scalars, vectors and tensors under spatial rotations, following the rules of coordinate transformations.

Taking all of these restrictions into account, the possible terms in the metric are introduced in the following way (Will, 2018):

1. g_{00} **to** $\mathcal{O}(2)$: Equation (4.8) defines a new Newtonian potential :

$$U(t, \boldsymbol{r}) := \int \frac{\rho^*(t, \boldsymbol{r})}{|\boldsymbol{r} - \boldsymbol{r'}|} d^3r', \tag{4.16}$$

where the conserved system's density $\rho^* = \rho\sqrt{-g}\,u^0$ satisfies Euler's continuity equation with u^0 as the time component of the four velocity. This potential satisfies a Poisson equation given by: $\nabla^2 U = -4\pi\rho^*$.

2. g_{jk} to $\mathcal{O}(2)$: Since g_{ik} is a 3D tensor, it is expected that generalized potentials of the form:

$$U_{\rm jk}(t,\boldsymbol{r}) := \int \rho(t,\boldsymbol{r})\frac{(r-r')_j(r-r')_k}{|\boldsymbol{r}-\boldsymbol{r'}|^3}d^3r', \tag{4.17}$$

must appear at $\mathcal{O}(2)$ in the expansion of g_{ik}.

3. g_{0j} to $\mathcal{O}(4)$: The only potentials that these components allow are of the form V_j and W_j which are 3D vectors given by:

$$\begin{aligned} V_j &:= \int \rho^*(t,\boldsymbol{r})\frac{v'_j}{|\boldsymbol{r}-\boldsymbol{r'}|}d^3r', \qquad\qquad \text{with: } \nabla^2 V_j = -4\pi\rho^* v_j. \\ W_j &:= \int \rho^*(t,\boldsymbol{r})\frac{\boldsymbol{v'}\cdot(\boldsymbol{r}-\boldsymbol{r'})(r-r')_j}{(|\boldsymbol{r}-\boldsymbol{r'}|)^3}d^3r', \end{aligned} \tag{4.18}$$

Note that these two vectors are related to each other through the *superpotential* X defined by:

$$X(t,\boldsymbol{r}) := \int \rho^*(t,\boldsymbol{r})\big|\boldsymbol{r}-\boldsymbol{r'}\big|d^3r'. \tag{4.19}$$

in the following manner:

$$X_{,0j} = W_j - V_j. \tag{4.20}$$

4. g_{00} to $\mathcal{O}(4)$: In this case the metric behaves as a scalar space, its components transform as scalars in any coordinate system and under any rotations. Taking all this into consideration, the following potentials are defined:

$$\Phi_1 := \int \rho^{*\prime}\frac{v'^2}{|\boldsymbol{r}-\boldsymbol{r'}|}\mathrm{d}^3r', \qquad \text{with } \nabla^2\Phi_1 = -4\pi\rho^* v^2, \tag{4.21}$$

$$\Phi_2 := \int \rho^{*\prime}\frac{U'}{|\boldsymbol{r}-\boldsymbol{r'}|}\mathrm{d}^3r', \qquad \text{with } \nabla^2\Phi_2 = -4\pi\rho^* U, \tag{4.22}$$

$$\begin{aligned} \Phi_3 &:= \int \rho^{*\prime}\frac{\Pi'}{|\boldsymbol{r}-\boldsymbol{r'}|}\mathrm{d}^3r', \qquad \text{with } \nabla^2\Phi_3 = -4\pi\rho^*\Pi, \\ \Phi_4 &:= \int \frac{p'}{|\boldsymbol{r}-\boldsymbol{r'}|}\mathrm{d}^3r', \qquad \text{with } \nabla^2\Phi_4 = -4\pi p, \\ \Phi_5 &:= \int \rho^{*\prime}\boldsymbol{\nabla}'U'\cdot\frac{(\boldsymbol{r}-\boldsymbol{r'})}{|\boldsymbol{r}-\boldsymbol{r'}|}\mathrm{d}^3r', \\ \Phi_6 &:= \int \rho^{*\prime}\frac{[\boldsymbol{v'}\cdot(\boldsymbol{r}-\boldsymbol{r'})]^2}{|\boldsymbol{r}-\boldsymbol{r'}|^3}\mathrm{d}^3r', \\ \Phi_W &:= \int\int \rho^{*\prime}\rho^{*\prime\prime}\frac{(\boldsymbol{r}-\boldsymbol{r'})}{|\boldsymbol{r}-\boldsymbol{r'}|^3}\cdot\left[\frac{(\boldsymbol{r'}-\boldsymbol{r''})}{|\boldsymbol{r}-\boldsymbol{r''}|}-\frac{(\boldsymbol{r}-\boldsymbol{r''})}{|\boldsymbol{r'}-\boldsymbol{r''}|}\right]\mathrm{d}^3r'\mathrm{d}^3r'', \end{aligned} \tag{4.23}$$

These potentials are related to each other by the following relations:

$$\begin{aligned}
\nabla^2 X &= 2U, \\
X_{,jk} &= U\delta_{jk} - U_{jk}, \\
X_{,0j} &= W_j - V_j, \\
X_{,00} &= \Phi_1 + 2\Phi_4 - \Phi_5 - \Phi_6, \\
\Phi_W &= -U^2 - \Phi_2 - \nabla U \cdot \nabla X + \nabla \cdot \int \frac{\rho^{*\prime}}{|\boldsymbol{r}' - \boldsymbol{r}''|} \nabla' X' d^3 r', \\
V_{j,j} &= -U_{,0}.
\end{aligned} \tag{4.24}$$

The inclusion of the above potentials into the metric perturbation to order $\mathcal{O}(4)$ will introduce unknown proportionality parameters. In order to fix them in a unique way, a specific gauge is chosen by performing an infinitesimal coordinates transformation:

$$x^{\bar{\mu}} = x^{\mu} + \xi^{\mu}(x^{\mu}), \tag{4.25}$$

and so, the metric $\bar{g}_{\bar{\mu}\bar{\nu}}(x^{\bar{\gamma}}$ in these new coordinates is given by:

$$\bar{g}_{\bar{\mu}\bar{\nu}}(x^{\bar{\gamma}}) = \frac{\partial x^{\bar{\mu}}}{\partial x_{\alpha}} \frac{\partial \bar{\nu}}{\partial x_{\beta}} g_{\alpha\beta} = g_{\mu\nu}(x^{\gamma}) - (\xi_{\mu,\nu} + \xi_{\nu,\mu}) + \mathcal{O}\big(\xi^2\big). \tag{4.26}$$

Since the general relativistic effects in higher perturbation orders converge to the Newtonian limit when $v/c \to 0$, the post-Newtonian approximation must obey the following statements:

1. The quantity $\xi_{\mu,\nu} + \xi_{\nu,\mu}$ must be a post-Newtonian approximation and so, it should vanish in the limit $v/c \to 0$.

2. $\xi_{\mu,\nu} + \xi_{\nu,\mu}$ and $|\xi^{\mu}|/|x^{\mu}|$ must vanish as $r \to \infty$.

The gradient of the superpotential is the only quantity that satisfies the above statements, i.e.:

$$\xi_0 = \lambda_1 \chi_{,0}, \qquad\qquad \xi_j = \lambda_2 \chi_{,j}, \tag{4.27}$$

where $\lambda_{1,2}$ are constants of proportionality.

The use of the above PPN gauge means that the metric components have the following values (Chandrasekhar, 1965):

$$\begin{aligned}
\bar{g}_{\bar{0}\bar{0}} &= g_{00} - 2\lambda_1(\Phi_1 + 2\Phi_4 - \Phi_5 - \Phi_6) + 2\lambda_2(U^2 + \Phi_2 + \Phi_W), \\
\bar{g}_{\bar{0}\bar{j}} &= g_{0j} - (\lambda_1 + \lambda_2)\chi_{,0j}, \\
\bar{g}_{\bar{j}\bar{k}} &= g_{jk} - 2\lambda_2 \chi_{,jk},
\end{aligned}$$

which can be further reduced by using Chandrasekhar (1965) "standard post-Newtonian gauge", which takes the spatial terms of the metric as diagonal and isotropic for simplicity. The final result yields:

$$
\begin{aligned}
g_{00} &= -1 + 2\lambda U + 2(\Psi) - \beta U^2 + \mathcal{O}(6), \\
g_{0j} &= -\frac{1}{2}\left[4(1+\gamma) + \alpha_1\right] V_j - \frac{1}{2}\left[1 + \alpha_2 - \zeta_1 + 2\xi\right] X_{,0j} + \mathcal{O}(5), \\
g_{jk} &= (1 + 2\gamma U)\delta_{jk} + \mathcal{O}(4),
\end{aligned}
$$

with:

$$
\Psi = \frac{1}{2}(2\gamma+1+\alpha_3+\zeta_1-2\xi)\Phi_1 - (2\beta-1-\zeta_2-\xi)\Phi_2 + (1+\zeta_3)\Phi_3 + (3\gamma+3\zeta_4-2\xi)\Phi_4 - \frac{1}{2}(\zeta_1-2\xi)\Phi_6 - \xi\Phi_W .
$$

The PPN parameters $\gamma, \beta, \beta_1, \beta_2, \beta_3, \beta_4, \xi, \eta, \Delta_1$ and Δ_2 as well as their Solar system values are shown in Figure (4.1)

Box 39.2 HEURISTIC DESCRIPTION OF THE TEN PPN PARAMETERS

Parameter	What it measures, relative to general relativity[a]	Value in General Relativity	Value in Dicke-Brans-Jordan Theory[b]	Value in Ni's Theory[b]
γ	How much space curvature (g_{jk}) is produced by unit rest mass?	1	$\frac{1+\omega}{2+\omega}$	1
β	How much nonlinearity is there in the superposition law for gravity (g_{00})?	1	1	1
β_1	How much gravity (g_{00}) is produced by unit kinetic energy ($\frac{1}{2}\rho_0 v^2$)?	1	$\frac{3+2\omega}{4+2\omega}$	1
β_2	How much gravity (g_{00}) is produced by unit gravitational potential energy ($\rho_0 U$)?	1	$\frac{1+2\omega}{4+2\omega}$	1
β_3	How much gravity (g_{00}) is produced by unit internal energy ($\rho_0 \Pi$)?	1	1	1
β_4	How much gravity (g_{00}) is produced by unit pressure (p)?	1	$\frac{1+\omega}{2+\omega}$	1
ζ	How much *more* gravity (g_{00}) is produced by radial kinetic energy $[\frac{1}{2}\rho_0(\mathbf{v}\cdot\hat{\mathbf{r}})^2]$—i.e., kinetic energy of motion toward observer—than by transverse kinetic energy?	0	0	0
η	How much *more* gravity (g_{00}) is produced by radial stress $[\hat{\mathbf{r}}\cdot\mathbf{t}\cdot\hat{\mathbf{r}}]$ than by transverse stress?	0	0	0
Δ_1	How much dragging of inertial frames (g_{0j}) is produced by unit momentum ($\rho_0 v$)?	1	$\frac{10+7\omega}{14+7\omega}$	$-\frac{1}{7}$
Δ_2	How much easier is it for momentum ($\rho_0 v$) to drag inertial frames radially (toward the observer) than in a transverse direction?	1	1	1

[a] These heuristic descriptions are based on equations (39.23).
[b] For expositions of these theories see Box 39.1. For derivation of their PPN values and of PPN values for other theories, see Ni (1972).

Figure 4.1: Description of each of the ten PPN parameters and their corresponding values for general relativity and two extended theories of gravity: Dicke-Brans-Jordan theory and Ni's theory (Table taken from: Misner et al., 1973).

§4.5 MONDian parametrization in spherical symmetry

A Tully-Fisher approach with relativity was the next step towards explaining the anomalies in the rotation curves of clusters of galaxies, given that the velocity dispersion in the outer regions of such are as small as 10^{-4}c, an approximation up to $\mathcal{O}(4)$ post-MONDian corrections is suitable for this model (Bernal et al., 2019a)*. To find the MONDian metric at $\mathcal{O}(2)$ of approximation, Mendoza & Olmo (2015) assumed the Einstein Equivalence Principle to hold and took the corresponding Tully-Fisher equation defined in Section §3.5.

The metric component g_{00} is obtained directly from the Tully-Fisher law for the motion of massive particles, whereas g_{11} is determined by the motion of massless particles i.e. photons (Bernal et al., 2019a). In order to show how this can be achived note that the metric components in spherical symmetry are given by:

$$\begin{aligned} g_{00} &= {}^{(0)}g_{00} + {}^{(2)}g_{00} + {}^{(4)}g_{00} + \mathcal{O}(6) = 1 + 2\phi/c^2 + {}^{(4)}g_{00} + \mathcal{O}(6), \\ g_{11} &= {}^{(0)}g_{11} + {}^{(2)}g_{11} + \mathcal{O}(4) = -1 + {}^{(2)}g_{11} + \mathcal{O}(4), \\ g_{22} &= -r^2, \\ g_{33} &= -r^2\sin^2\theta, \end{aligned} \tag{4.28}$$

where $\phi = -U$ is the non-relativistic gravitational potential. Note that at $\mathcal{O}(0)$ of approximation, space-time is flat Minkowski and so the metric components ${}^{(0)}g_{00}$ and ${}^{(0)}g_{11}$ are given by the results of equation (4.5).

Using the results of equations (4.28) it follows that the acceleration a at perturbation order O(4) is given by (see appendix §5.4):

$$\frac{1}{c^2}a = \frac{1}{c^2}\frac{\mathrm{d}^2 r}{\mathrm{d}t^2} = \frac{1}{2}\left[\frac{\mathrm{d}^{(2)}g_{00}}{\mathrm{d}r} + {}^{(2)}g_{11}\frac{\mathrm{d}^{(2)}g_{00}}{\mathrm{d}r} + \frac{\mathrm{d}^{(4)}g_{00}}{\mathrm{d}r}\right]. \tag{4.29}$$

We now describe how to obtain the metric components up to the required perturbation orders.

At $\mathcal{O}(2)$ of approximation, the PPN MONDian corrections were obtained by Bernal et al. (2019a); Mendoza & Olmo (2015); Mendoza (2015b, 2023) in the following manner:

$$g_{00} = 1 + \frac{2\phi}{c^2} = 1 - \frac{2}{c^2}\left(\sqrt{GMa_0}\ln(r/r_*)\right), \tag{4.30}$$

$$g_{11} = 1 + \frac{2r}{c^2}\frac{\mathrm{d}\phi}{\mathrm{d}r} = 1 - \frac{2}{c^2}\sqrt{GMa_0}. \tag{4.31}$$

With these results, the acceleration (4.29) at $\mathcal{O}(2)$ of approximation is given by:

$$a = \frac{\mathrm{d}^{(2)}g_{00}}{\mathrm{d}r} = -\frac{\sqrt{GMa_0}}{r}. \tag{4.32}$$

*At first sight, the fact that 10^{-4}c is indeed a small quantity to be taken into account, it is important to mention the following fact. The planet Mercury, rotates about the Sun at a speed of $\sim 1.6\times10^{-4}$c and its general relativistic corrections of its Newtonian description at $\mathcal{O}(4)$ of approximation yield the rotation of its perihelium (see e.g. Landau, 2013; Will, 2018). It is thus expected that the that relativistic corrections to MONDian dynamics are needed to explain the dynamics of clusters of galaxies.

.

When dealing with a spherical mass distribution $M(r)$, Mendoza et al. (2011) showed from very general dimensional arguments that the previous equation is valid also by the substitution $M \to M(r)$[†].

Now, since the metric component ${}^{(2)}g_{11}$ is dimensionless, then by Buckingham's Π-theorem of dimensional analysis, its more general form should be given by:

$$ {}^{(2)}g_{11} = -\frac{\sqrt{Ga_0}}{c^2} \times \mu(r)^{1/2}, $$

where the function $\mu(r)$ is a function that has dimensions of mass. When dealing with a point mass M particle, equation (4.31) shows that $\sqrt{\mu(r)} = 2\sqrt{M}$. It is natural to expect then that $\mu(r) \propto M(r)$ for a spherical distribution of matter, i.e.:

$$ {}^{(2)}g_{11} = -\frac{\alpha_1}{c^2}\sqrt{GM(r)a_0}, \tag{4.34} $$

where α is a dimensionless quantity.

Substitution of equation (4.34) and (4.32) into (4.29) yields:

$$ a = -\frac{\sqrt{GM(r)a_0}}{r} + \frac{\alpha_1}{c^2}\frac{GM(r)a_0}{r} + c^2\frac{\mathrm{d}^{(4)}g_{00}}{\mathrm{d}r} \tag{4.35} $$

In principle, we expect α_1 to be constant, but since it comes from dimensional groundings one should also consider:

$$ \alpha_1 = a + B\ln(r/r_\star) = A + B\ln(r), \tag{4.36} $$

where $A = a - B\ln(r_\star)$, B and $r_\star$ are constant, so that

$$ a = -\frac{\sqrt{M(r)a_0}}{r} + (A + B\ln(r))\frac{GM(r)a_0}{r} + \frac{\mathrm{d}^{(4)}\phi}{\mathrm{d}r} \tag{4.37} $$

where ${}^{(4)}\phi := {}^{(4)}g_{00}c^2$. Once again, from dimensional goundings ${}^{(4)}\phi$ should be:

$$ \phi = -\frac{G\mu a_0}{c^2}(\lambda_1 + \lambda_2\ln(r)). \tag{4.38} $$

Since this particular form is basically expressed in the second term of the right-hand side of equation (4.37), then we can think of a further generalisation using the following argument. The PPN approach is essentially a linearisation of the potential fields. By allowing this to be

[†]Using Buckingham's Π-theorem of dimensional analysis, Mendoza et al. (2011) showed that if the dimensional constant a_0 is introduced into a non-relativistic description of gravity, then the acceleration a experienced by a test particle at a distance r from the origin is given by:

$$ a = a_0 f(x), \quad \text{where:} \quad x := l_M/r, \quad \text{and} \quad l_M := \sqrt{GM/a_0}. \tag{4.33} $$

As such, Newton's gravity is recovered when the function $f(x) = x^2$ and MOND's one when $f(x) = x$.

In order to see that the mass M can be substituted for $M(r)$ and so, it validates Newton's theorems (Mendoza, 2015a) suppose that $a \propto x^p$ with p an integer number and assume that a test particle is located at position r inside a spherically symmetric distribution contained within a radius R. If we trace a cone with solid angle $\delta\Omega$ and vertex at the test particle, the shell is intersected at two opposite points $\boldsymbol{r}_1$ and $\boldsymbol{r}_2$. The masses δM_1 and δM_2 contained within the solid angle $\delta\Omega$ at these points are such that $\delta M_2/\delta M_1 = (r_2/r_1)^2$. This relation means that $(\delta M_1/r_1^2)^{p/2} = (\delta M_2/r_2^2)^{p/2}$, and so $\delta x^p(r_1) = \delta x^p(r_2)$.

true, even at the fourth orther of approximation as expressed in the previous equation, then the general potential at this $\mathcal{O}(4)$ perturbation order is obtained by the convolution:

$$\phi = -\lambda \frac{Ga_0}{c^2} \int \frac{\rho' \, \mathrm{d}V'}{|\vec{r} - \vec{r}'|} - \frac{\lambda_2 G a_0}{c^2} \int \frac{\rho' \, \mathrm{d}V' \ln(|\vec{r} - \vec{r}'|)}{|\vec{r} - \vec{r}'|}. \tag{4.39}$$

And so:

$$\begin{aligned} \frac{\mathrm{d}\phi}{\mathrm{d}r} = &-\frac{\lambda_1 G a_0}{c^2} \, \mathrm{d}r \left[\int_0^r + \int_r^R \right] \left[\int_0^\pi \frac{\rho' r^2 \, \mathrm{d}r \, \mathrm{d}\theta \, 2\pi}{\sqrt{r^2 + r'^2 + rr' \cos(\theta)}} \right] \\ &- \frac{\lambda_2 G a_0}{c^2} \frac{\mathrm{d}}{\mathrm{d}r} \left[\int_0^r + \int_r^R \right] \left[\int_0^\pi \frac{\rho' r^2 \, \mathrm{d}r \, \mathrm{d}\theta \, 2\pi \ln(|\vec{r} - \vec{r}'|)}{\sqrt{r^2 + r'^2 + rr' \cos(\theta)}} \right], \end{aligned} \tag{4.40}$$

which yields:

$$\boxed{a = -\frac{\sqrt{GM(r)a_0}}{r} + (A^\star + B^\star \ln(r)) \frac{GM(r)a_0}{c^2 r},} \tag{4.41}$$

where $A^\star$ and $B^\star$ are dimensionless constants.

Chapter 5

Clusters of galaxies as probes for a relativistic MOND

The use of clusters of galaxies to calibrate a relativistic modified Newtonian dynamics (MOND) model is described in this chapter. It highlights the importance of clusters of galaxies as a calibration method because of their symmetry, structure, and size, which makes them easy to analyze. Clusters of galaxies have an intracluster medium (ICM) mainly made up of ionized hydrogen and helium, which emits radiation mostly in the X-ray spectrum. With this, the missing component in the cluster mass distribution can be determined by analyzing the temperature and gas profiles. The acceleration of the cluster radius concerning temperature and gravitational potential for a system in gravitational equilibrium is described. Finally, it is shown that mass particles of clusters of galaxies can be explained using only their baryonic mass and the MOND's fourth perturbation order results of the previous chapter.

§5.1 Theoretical mass

For astrophysical environments, the results of the previous Chapter can be immediately applied to sufficiently spherical clusters of galaxies in order to calibrate the unknown free parameters $A^\star$ and $B^\star$ of equation (4.41). Individual, groups and clusters of galaxies were all formed during a gravitational collapse from where gas clouds arose and cooled at different rates, allowing these massive bodies to form thanks to hydrostatic equilibrium. Clusters of galaxies have hot gas within them at temperatures $T \sim 10^7 - 10^8$ K, and are mainly made of an intracluster medium (ICM) of ionized hydrogen HII and helium He, which emits radiation mostly in the X-ray spectrum due to Bremsstrahlung (free-free) radiation (Sparke & Gallagher III, 2007).

Using X-ray telescopes, such as e.g. the Chandra observatory, mapping of the ICM temperature and mass profiles has been done to a very high accuracy on relaxed clusters that have almost reached their dynamical equilibrium (Vikhlinin et al., 2006). As seen in equation (4.41), the missing component is the $M(r)$ mass distribution and in Bernal et al. (2019a), the 11 clusters' temperature and gas profiles seen in Vikhlinin et al. (2006) were used to find this mass profile distribution and the parameter A, where, given the hydrostatic equilibrium and their weak dynamical activity, hence relaxed, an isotropic and very spherically symmetric

system is assumed.

Given all of the properties and composition of the ICM in clusters of galaxies, the ideal gas law and Boltzmann's equation, it is possible to describe the acceleration along their radius with respect to their temperature $T(r)$ and the gravitational potential Φ for a system in gravitational equilibrium as (Bernal et al., 2019a):

$$|\boldsymbol{a}(r)| = \left|\frac{\mathrm{d}\Phi(r)}{\mathrm{d}r}\right| = \frac{k_B T(r)}{\mu m_p}\left[\frac{\mathrm{d}\ln(\rho_g(r))}{\mathrm{d}\ln(r)} + \frac{\mathrm{d}\ln(T(r))}{\mathrm{d}\ln(r)}\right], \tag{5.1}$$

where μ is the He abundance's molecular mass per particle, m_p is the proton's mass and k_{B} represents Boltzmann's constant.

The mass of this system can then be defined by taking equation (2.4) and the total mass then compared to the theoretical mass $M_{\mathrm{th}}(r)$ given by the acceleration in equation (4.41). Since this model aims to account for the dark matter discrepancy then $M_{\mathrm{th}}(r) = M_{\mathrm{dyn}}(r)$. Note that the dark matter term M_{DM} was put aside in order to properly compare these two masses. Therefore, by taking the dynamical mass equation (2.3) and putting it in terms of the centripetal acceleration a_c:

$$M_{\mathrm{dyn}}(r) = -\frac{r^2 a_c(r)}{G} = -\frac{v^2 r}{G}. \tag{5.2}$$

For the observations, the acceleration $a_c(r)$ is given by the value derived in equation (5.1), which yields a dynamical mass of:

$$M_{\mathrm{dyn}}(r) = \frac{-r}{G}\frac{k_B T(r)}{\mu m_p}\left[\frac{\mathrm{d}\ln(\rho_g(r))}{\mathrm{d}\ln(r)} + \frac{\mathrm{d}\ln(T(r))}{\mathrm{d}\ln(r)}\right], \tag{5.3}$$

and for the theoretical mass the acceleration value of equation (4.41) yields:

$$\boxed{M_{\mathrm{th}}(r) = r\,\frac{(M(r)a_0)^{1/2}}{G^{1/2}} - \frac{rM(r)a_0}{c^2}(A^\star + B^\star \ln(r)),} \tag{5.4}$$

where $M(r) = M_{\mathrm{gas}}(r) + M_{\mathrm{stars}}(r)$ is the baryonic mass $M_b(r)$ of the cluster. Which is composed of a gas-mass component M_{gas} plus a star-mass component M_{stars}

§5.2 Sample of clusters

The baryonic mass $M_b(r)$ needed can be calculated from the observations by analyzing the baryonic density $\rho_g(r)$ of the gas in each cluster. This in turn is dependent on the entire gas density distribution and so, it is a function of the temperature profiles $T(r)$ as well. These temperature profiles were taken from 11 clusters of galaxies with primordial He abundance at a low red-shift z=$0.01 - 0.2$ with a median of $z = 0.06$ in order to exclude the effects of the universe's expansion. These were also taken at around $0.75r_{500}$, from where Vikhlinin et al. (2006) then measured the surface brightness of the clusters at the $0.7 - 2$ keV energy band with a projected metallicity of $Z = 0.2Z_\odot$.

Starting with the gas density distribution, a β probability distribution model was used with a small modification, which in the case of these types of clusters, must be led by a power law with respect to the radius. A second β parameter was added to the model in order to add

detail and accuracy within a small radius near the center (Vikhlinin et al., 2006). Finally, the emission profile was fitted to the 11 clusters using:

$$n_p n_e = \frac{n_0^2 (r/r_c)^{-\alpha}}{(1+r^2/r_c^2)^{3\beta-\alpha/2}(1+r^\gamma/r_s^\gamma)^{\epsilon/\gamma}} + \frac{n_{02}^2}{(1+r^2/r_{c2}^2)^{3\beta_2}}, \tag{5.5}$$

which yielded the values for the parameters $n_0, r_c, r_s, \alpha, \beta, \epsilon, n_{02}, r_{c2}, \beta_2, \gamma = 3$ in the equation.

For these types of clusters with the composition described above, the gas density can be defined by:

$$\rho_g = 1.624 m_p (n_p n_e)^{1/2}. \tag{5.6}$$

For the temperature profile, Vikhlinin et al. (2006) showed a decrease in temperature towards the center of the clusters and therefore, derived an analytical three dimensional solution for this change in temperatures $T(r) = T_{\rm oc}(r)\ T_{\rm cool}(r)\ T_0$. Outside of the region with the decrease of temperature (assumed to be radiation cooling) the temperature was defined by

$$T_{\rm oc}(r) = \frac{(r/r_t)^{-a}}{[1+(r/r_t)^b]^{c/b}}, \tag{5.7}$$

where r_t is the point in which the temperature transitions from one state to the other. Inside of the cooling region, the following relation was derived:

$$T_{\rm cool}(r) = \frac{[(r/r_{\rm cool})^{a_{\rm cool}} + T_{\rm min}/T_0]}{[(r/r_{\rm cool})^{a_{\rm cool}} + 1]}, \tag{5.8}$$

Finally, the 3D temperature profile was calibrated using the equation:

$$T(r) = T_0\ \frac{(r/r_t)^{-a}}{[1+(r/r_t)^b]^{c/b}}\ \frac{[(r/r_{\rm cool})^{a_{\rm cool}} + T_{\rm min}/T_0]}{[(r/r_{\rm cool})^{a_{\rm cool}} + 1]}, \tag{5.9}$$

Vikhlinin et al. (2006) were also able to find these parameters $a, b, c, r_t, T_0, T_{min}, r_{cool}, a_{cool}$.

Having all the needed values and formulas in order to calculate the baryonic and theoretical masses, Bernal et al. (2019a) used the empirical relationship between the total mass of the system at r_{500} and the stellar mass given by:

$$\frac{M_{stars}}{10^{12} M_\odot} = (1.8 \pm 0.1) \left(\frac{M_{500}}{10^{14} M_\odot} \right)^{0.71 \pm 0.04}. \tag{5.10}$$

Given the previous information, the stellar mass of the galaxy clusters is more or less 1% of the total mass and therefore can be neglected, allowing the dynamical mass of the gas component to be the baryonic mass. The dynamical mass M_{dyn} was calculated for each of the radial points given for each of the clusters by using equation (5.3) and the values for the constants:

$$
\begin{aligned}
k_B &= 1.380\,648\,52 \times 10^{23}\,\mathrm{kg\,s^{-2}\,K^{-1}},\\
m_p &= 1.672\,621\,89 \times 10^{-27}\,\mathrm{kg},\\
G &= 6.674 \times 10^{-11}\,\mathrm{m^3\,kg^{-1}\,s^{-2}},\\
\mu &= 0.609.
\end{aligned}
$$

Bernal et al. (2019b) used the data provided by Alexey Vikhlinin to fit their model.

This same data was used in this work. The data given was set up for each of the 11 galaxy clusters in the same way: radius, density, gas mass, temperature, dynamical mass and pressure, and with their corresponding uncertainties.

The given data was converted by a script in order to have it in units of megaparsecs for distances, and normalized to $10^{14} M_\odot$.

§5.3 Statistical Fit

§5.3.1 Parameters $A^\star$ and $B^\star$

In order to fit the parameters $A^\star$ and $B^\star$ to their best approximation using the theoretical mass equation $M_{th}(r)$, the "fit" GNUplot (Williams & Kelley, 2020) fitting function was used, which uses a nonlinear least-squares (NLLS) Marquardt-Levenberg algorithm. This algorithm combines the gradient descent method, which minimizes errors using a steep descent direction for solutions far from optimization and the Gauss-Newton method, which minimized errors by finding the minimum assuming a locally quadratic least squares function for solutions close to optimization (Gavin, 2019).

§5.4 Results

Table §5.4 shows the best fitting values of the parameters using the routine described in the previous section. The values $r_{\min}$ and $r_{\max}$ represent the lower and upper values of the radius used for the fitting in equation (5.4).

The following figures show the corresponding fits made for each of the clusters with distance in units of megaparsecs, and mass in units of and $10^{14} M_\odot$.

The figures on the right show the fit made for the gas mass with the M_g from the observations in red and the mass fit $M(r)$ for the clusters in blue.

Putting the two previous values together into the figures on the left, the dynamical mass $M_{\mathrm{dyn}}(r)$ calculated in (5.3) is in red and the theoretical mass M_{th} fit calculated in (5.4) is shown in blue.

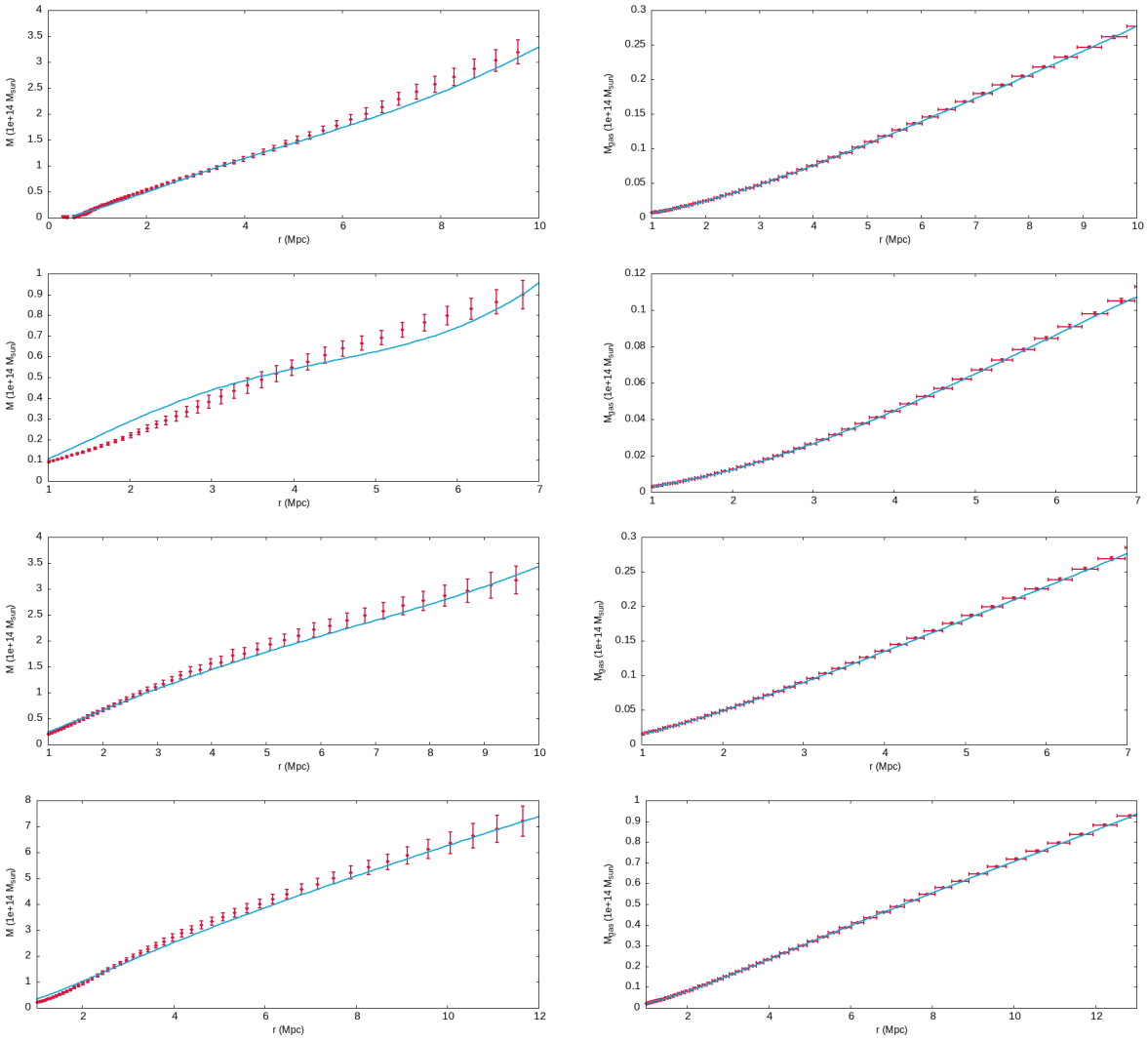

Figure 5.1: On the left, the theoretical mass fits between the observational data (in red) with its corresponding error bars and the derived expressions for the galaxy clusters A133, A262, A383 and A478 (in blue) are seen from top to bottom in that order. On the right Gas mass fit in blue fits perfectly with respect to the radius and the observational mass in red.

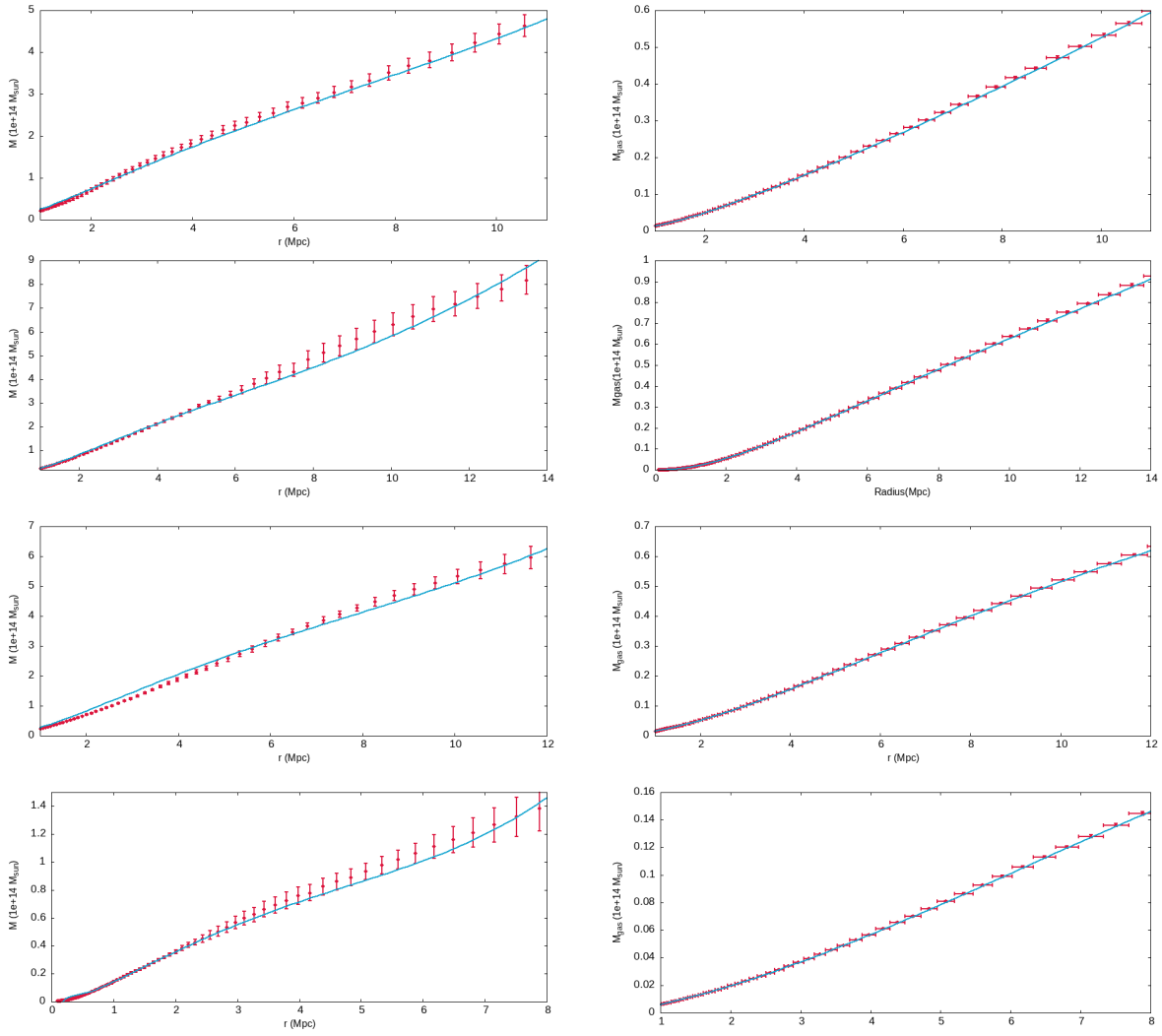

Figure 5.2: On the left, the theoretical mass fits between the observational data (in red) with its corresponding error bars and the derived expressions for the galaxy clusters A907, A1413, A1795 and A1991 (in blue) are seen from top to bottom in that order. On the right Gas mass fit in blue fits perfectly with respect to the radius and the observational mass in red.

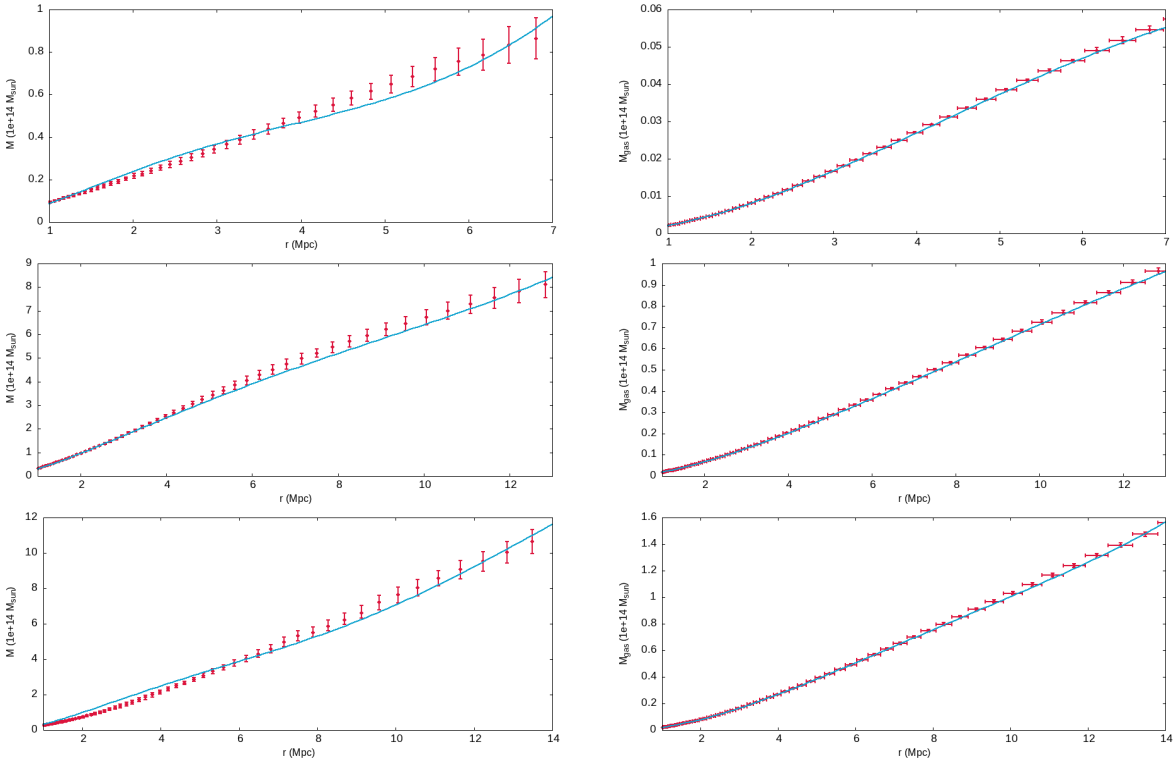

Figure 5.3: On the left, the theoretical mass fits between the observational data (in red) with its corresponding error bars and the derived expressions for the galaxy clusters MKW4, A2029 and A2390 (in blue) are seen from top to bottom in that order. On the right Gas mass fit in blue fits perfectly with respect to the radius and the observational mass in red.

Cluster	r_{min} (Mpc)	r_{max} (Mpc)	$A^\star$	$B^\star$
A133	0.3148	12.8370	2.6231e-10	-6.7228e-11
A262	0.5654	10.0581	4.5893e-10	-1.3908e-10
A383	0.1246	11.6436	1.8966e-10	-4.2748e-11
A478	0.5128	14.8605	1.1131e-10	-2.0622e-11
A907	0.6233	14.8605	1.6873e-10	-3.8959e-11
A1413	0.4429	14.8605	1.3989e-10	-3.1178e-11
A1795	1.0154	14.8605	1.3992e-10	-2.7829e-11
A1991	0.2720	12.8370	3.5922e-10	-9.7040e-11
MKW4	0.4018	9.5792	5.4701e-10	-1.5547e-10
A2029	0.4884	13.4789	1.1863e-10	-2.4104e-11
A2390	0.3645	14.8605	1.2346e-10	-2.9941e-11
		Average	2.3810e-10	-6.1291e-11
		Avg. std. error	2.64e-12	1.495e-12

Table 5.1: Parameters shown in this table are taken from the fits of equation (5.4) to the observational data of the 11 clusters of galaxies as described in the text. The average value and the average standard error for the parameters $A^\star$ and $B^\star$ are also shown.

Conclusions

The concept of mass-to-light ratio has been very useful in calculating the mass of galaxies. This ratio is related to the age of the populations of stars within the galaxy and its visible light, and is used to determine the amount of "undetected" mass or dark matter within a galaxy. The development of rotation curves of spiral galaxies in the 1960s and 1970s was critical in establishing the role of the mass-to-light ratio, and the discovery of dark matter. The mass of clusters of galaxies can be determined by analyzing their rotational velocities, as well as through X-ray observations and gravitational lensing. Understanding the distribution of mass within galaxies and clusters is essential to understanding the structure and evolution of the universe.

This thesis discusses the evolution of gravity-related concepts from the 17th to the 19th century. Descartes introduced the idea of occult fluids in 1644 to explain that empty space could not exist and space must contain something similar to a body. Newton built on these ideas and formulated the idea of gravity as a force in his Principia. Kepler's Harmonices Mundi Libri IV provided important information on the patterns of planetary motion, which led to the third law of planetary motion, $T^2 \propto a^3$. LeVerrier and Adams predicted Neptune's existence, and their calculations led to its discovery beyond Uranus in 1845. These discoveries and theories paved the way for modern concepts of gravity, including Einstein's General Relativity.

This thesis also discusses the Einstein Equivalence Principle (EEP), which states that the outcome of any experiment would be independent of its place or time in the universe as long as the Weak Equivalence Principle (WEP) is valid. The WEP implies that the inertial and gravitational mass of bodies would be the same during free fall, and this principle could be extended to all laws of physics. The principle of least action is also introduced, which yields the equations of motion of a test particle in a system, and the geodesic trajectory of such a particle is described by requiring a functional action to reach a minimum value. The author also discusses the Lagrangian of the system and the metric tensor, which is used to describe the interval between two infinitesimal points in a curved space-time. Additionally, the author introduces the concept of PPN parameters, which are used to parameterize deviations from general relativity.

In conclusion, galaxy clusters can be used as a calibration method to study dark matter and modified gravity theories. X-ray telescopes like the Chandra observatory have provided high-accuracy mapping of the intracluster medium (ICM) temperature and mass profiles of relaxed clusters of galaxies, which are assumed to be isotropic and spherically symmetric. By taking into account the properties and composition of ICM and using the ideal gas law and

Boltzmann's equation, it is possible to describe the acceleration of the system in gravitational equilibrium with respect to its temperature and gravitational potential. Using the dynamical mass equation, the baryonic mass of the cluster can be calculated from the observations of the baryonic density and temperature profiles of the gas in each cluster. A β probability distribution model with a power law and a second β parameter was used to fit the emission profile of the 11 clusters studied. The resulting data was used to find the mass profile distribution and the parameters $A^\star$ and $B^\star$, which accounts for the dark matter discrepancy.

As seen in each of the figures in chapter 5 the calculated theoretical mass $M_{\rm th}$ was fitted to the best of the possibilities to the observational data within the MOND limit to a fourth order perturbation in order to seek better accuracy and to show that a Tully-Fisher based MOND theory works well with the aforementioned observational data.

Theoretical gas density and gas mass were fitted well into the observations and are within the limits of each of these values' uncertainties.

As with the $M_{\rm th}$, the fits are for the most part within the uncertainties of the observational calculated values and their uncertainties. Therefore, one can conclude that the approximations of the model seen in this work are a good match. One can see that when a higher order perturbation is taken, a small value for the free unknown parameters $A^\star$ and $B^\star$ seen in table §5.4 are different to model clusters of galaxies mass profiles.

Appendix

Using the geodesic equation:

$$\frac{\mathrm{d}^2 x^\alpha}{\mathrm{d}\tau^2} + \mathcal{T}^\alpha_{\beta\zeta}\frac{\mathrm{d}x^\beta}{\mathrm{d}\tau}\frac{\mathrm{d}x^\zeta}{\mathrm{d}\tau} = 0, \tag{11}$$

where $\alpha = 1 = r$, $\ddot{r} = 0$, $\dot{r} = 0$ and $\dot{\theta} = 0$ therefore

$$c^2\mathcal{T}^1_{00}\dot{t}^2 + 2\mathcal{T}^1_{03}\dot{t}\dot{\varphi} + \mathcal{T}^1_{33}\dot{\varphi}^2 = 0. \tag{12}$$

Taking each $\mathcal{T}^\alpha_{\beta\zeta}$ term on their own:

$$\begin{aligned}\mathcal{T}^1_{00} &= \frac{1}{2}g^{1\lambda}\left[\frac{\partial g_{0\lambda}}{\partial x^0} + \frac{\partial g_{0\lambda}}{\partial x^0} - \frac{\partial g_{00}}{\partial x^\lambda}\right], \\ &= \frac{1}{2}g^{11}\left(-\frac{\partial g_{00}}{\partial r}\right),\end{aligned} \tag{13}$$

$$\begin{aligned}\mathcal{T}^1_{03} &= \frac{1}{2}g^{1\lambda}\left[\frac{\partial g_{0\lambda}}{\partial x^3} + \frac{\partial g_{3\lambda}}{\partial x^0} - \frac{\partial g_{03}}{\partial x^\lambda}\right], \\ &= \frac{1}{2}g^{11}\,(0) = 0,\end{aligned} \tag{14}$$

$$\begin{aligned}\mathcal{T}^1_{33} &= \frac{1}{2}g^{1\lambda}\left[\frac{\partial g_{3\lambda}}{\partial x^3} + \frac{\partial g_{3\lambda}}{\partial x^3} - \frac{\partial g_{33}}{\partial x^\lambda}\right], \\ &= \frac{1}{2}g^{11}\left(-\frac{\partial g_{33}}{\partial x^1}\right) = \frac{1}{2}(2r),\end{aligned} \tag{15}$$

Substituting equations (13), (14), (15) into equation (12) yields:

$$-\frac{\partial g_{00}}{\partial r}\dot{t}^2c^2 + 2e\dot{\varphi}^2 = 0 \tag{16}$$

Now, taking

$$\begin{aligned}c^2 = \frac{\mathrm{d}s^2}{\mathrm{d}\tau^2} &= c^2\frac{\mathrm{d}t^2}{\mathrm{d}\tau^2}g_{00} + g_{11}\frac{\mathrm{d}r^2}{\mathrm{d}\tau^2} - r^2\frac{\mathrm{d}\varphi^2}{\mathrm{d}\tau^2}, \\ &= c^2\dot{t}^2g_{00} + g_{11}\dot{r}^2 - r^2\dot{\varphi}^2,\end{aligned}$$

since $\dot{r} = 0$ the second term disappears and the previous equation is then

$$\dot{t}^2 = \frac{1}{c^2}(c^2 + r^2\varphi^2). \tag{17}$$

Substituting equation (17) into equation (16) and using $v = r\dot{\varphi}$ yields:

$$\begin{aligned}
&\frac{-c^2 g_{00,r}}{c^2 g_{00}}\left(c^2 + r^2\dot{\varphi}^2\right) + 2r\dot{\varphi}^2 = 0,\\
&= \frac{-g_{00,r}}{g_{00}}\left(c^2 + v^2\right) + 2\frac{v^2}{r} = 0,\\
&= \frac{-c^2 g_{00,r}}{g_{00}} + \frac{v^2}{r}\left[2 - \frac{-r g_{00,r}}{g_{00}}\right],\\
\frac{v^2}{r} &= \frac{-c^2 g_{00,r}}{2g_{00}}\frac{1}{1 - \frac{-r g_{00,r}}{2g_{00}}},
\end{aligned} \tag{18}$$

and in the observer's frame:

$$\frac{v^2}{r} = \frac{-c^2 g_{00,r}}{2}\frac{1}{1 - \frac{-r g_{00,r}}{2g_{00}}}. \tag{19}$$

Using

$$g_{00} = 1 + {}^{(2)}g_{00} + {}^{(4)}g_{00}, \tag{20}$$

and

$$g_{00,r} = {}^{(2)}g_{00,r} + {}^{(4)}g_{00,r}, \tag{21}$$

the following equation can be derived:

$$\begin{aligned}
r\frac{g_{00,r}}{g_{00}} &= r({}^{(2)}g_{00,r} + {}^{(4)}g_{00,r})(1 - {}^{(2)}g_{00} - {}^{(4)}g_{00}),\\
&= r{}^{(2)}g_{00,r}{}^{(2)}g_{00} + r{}^{(4)}g_{00,r}.
\end{aligned} \tag{22}$$

Finally, the substitution of this last result into equation (18) yields:

$$\frac{v^2}{r} = \frac{c^2}{2}\left[{}^{(2)}g_{00,r} + {}^{(4)}g_{00,r} + \frac{1}{2}{}^{(2)}g_{00,r}{}^{(2)}g_{00,r}r\right]. \tag{23}$$

Bibliography

Bekenstein, J., 2005. Relativistic gravitational theory for the MOND paradigm. *Phys. Rev. D*, **70**.

Bekenstein, J. & Milgrom, M., 1984. Does the missing mass problem signal the breakdown of Newtonian gravity? *The Astrophysical Journal*, **286**, 7–14.

Bernal, T., López-Corona, O. & Mendoza, S., 2019a. Dynamics of clusters of galaxies with extended f (χ)= χ 3/2 gravity. *arXiv preprint arXiv:1505.00037*.

Bernal, T., López-Corona, O. & Mendoza, S., 2019b. Dynamics of clusters of galaxies with extended F (χ) gravity. *Revista mexicana de astronomía y astrofísica*, **55**(2), 237–254.

Burbidge, E. M., Burbidge, G. & Prendergast, K., 1961. The Rotation and Mass of NGC 157. *The Astrophysical Journal*, **134**, 874.

Capozziello, S. & De Laurentis, M., 2011. Extended theories of gravity. *Physics Reports*, **509**(4-5), 167–321.

Chandrasekhar, S., 1965. Astrophysical constraints and insights on extended relativistic gravity. ApJ, **357**(2), 133.

Durrer, R., 2020. *The cosmic microwave background*. Cambridge University Press.

Fabian, A., Arnaud, K. & Thomas, P., 1987. Cooling flows and the formation of dark matter. In *Symposium-International astronomical union*, vol. 117, 201–213. Cambridge University Press.

Famaey, B. & Binney, J., 2005. Modified Newtonian dynamics in the Milky Way. MNRAS, **363**(2), 603–608.

Fontenrose, R., 1973. In search of Vulcan. *Journal for the History of Astronomy*, **4**(3), 145–158.

Gavin, H. P., 2019. The Levenberg-Marquardt algorithm for nonlinear least squares curve-fitting problems. *Department of Civil and Environmental Engineering, Duke University http://people. duke. edu/˜ hpgavin/ce281/lm. pdf*, 1–19.

Gingerich, O., 1975. 10.9. The origins of Kepler's Third Law. *Vistas in astronomy*, **18**, 595–601.

Hoekstra, H., Bartelmann, M., Dahle, H., Israel, H., Limousin, M. & Meneghetti, M., 2013. Masses of galaxy clusters from gravitational lensing. *Space Science Reviews*, **177**(1-4), 75–118.

Jarrell, R. A., 2007. *Bouvard, Alexis*. Springer New York, New York, NY.

Landau, L. & Lifshitz, E., 1976. *CHAPTER I - THE EQUATIONS OF MOTION*. Butterworth-Heinemann, Oxford, third edition ed. ISBN 978-0-7506-2896-9. URL https://www.sciencedirect.com/science/article/pii/B978008050347950006X.

Landau, L. D., 2013. *The classical theory of fields*, vol. 2. Elsevier.

Lars, B., Eliezer, R., Khoo, P. K. et al., 2019. *Jacob Bekenstein: The Conservative Revolutionary*. World Scientific.

McGaugh, S. S., Schombert, J. M., Bothun, G. D. & De Blok, W., 2000. The baryonic tully-fisher relation. *The Astrophysical Journal Letters*, **533**(2), L99.

Melia, F., 2022. The Friedmann–Lemaître–Robertson–Walker metric. *Modern Physics Letters A*, **37**(03), 2250016.

Mendoza, S., 2015a. *Astrofisica Relativista*. URL https://mendozza.org/sergio/gravitacion/astro-rel.pdf.

Mendoza, S., 2015b. MOND as the basis for an extended theory of gravity. *Canadian Journal of Physics*, **93**(2), 217–231.

Mendoza, S., 2023. Metric tensor at second perturbation order for spherically symmetric space-times. *International Journal of Geometric Methods in Modern Physics*. URL https://doi.org/10.1142/s0219887823501074.

Mendoza, S., Hernández, X., Hidalgo, J. C. & Bernal, T., 2011. A natural approach to extended Newtonian gravity: tests and predictions across astrophysical scales. *Monthly Notices of the Royal Astronomical Society*, **411**(1), 226–234.

Mendoza, S. & Olmo, G. J., 2015. Astrophysical constraints and insights on extended relativistic gravity. *Astrophysics and Space Science*, **357**(2), 133.

Mendoza, S. & Silva, S., 2021. The matter Lagrangian of an ideal fluid. *International Journal of Geometric Methods in Modern Physics*, **18**(04), 2150059. URL https://doi.org/10.1142%2Fs0219887821500596.

Milgrom, M., 1983. A modification of the Newtonian dynamics as a possible alternative to the hidden mass hypothesis. *The Astrophysical Journal*, **270**, 365–370.

Miller, R., 1984. *René Descartes: Principles of Philosophy: Translated, with Explanatory Notes*, vol. 24. Springer Science & Business Media.

Misner, C. W., Thorne, K. S., Wheeler, J. A. et al., 1973. *Gravitation*. Macmillan.

Newton, I., 1729. *The Mathematical Principles of Natural Philosophy*. The Mathematical Principles of Natural Philosophy. B. Motte, 3rd ed. URL `http://books.google.es/books?id=TmOFAAAAQAAJ`.

Paterno-Mahler, R., Blanton, E., Brodwin, M., Ashby, M., Golden-Marx, E., Decker, B., Wing, J. & Anand, G., 2017. The High-redshift Clusters Occupied by Bent Radio AGN (COBRA) Survey: The Spitzer Catalog. *The Astrophysical Journal*, **844**(1), 78.

Perlmutter, S. et al., 2003. Supernovae, dark energy, and the accelerating universe. *Physics today*, **56**(4), 53–62.

Puget, J.-L., 2021. The Planck Mission and the Cosmic Microwave Background. In *The Universe*, 73–92. Springer.

Salucci, P. & Persic, M., 1997. Dark matter halos around galaxies. *arXiv preprint astro-ph/9703027*.

Smart, W. M., 1947. John Couch Adams and the discovery of Neptune. *Popular Astronomy*, **55**, 301.

Smith, S., 1936. The mass of the Virgo cluster. *The Astrophysical Journal*, **83**, 23.

Sparke, L. S. & Gallagher III, J. S., 2007. *Galaxies in the universe: an introduction*. Cambridge University Press.

Spratt, J.-S., 2016. The Descartes-Newton paradox: Clashing theories of planetary motion at the turn of the eighteenth century.

Tkachev, I., 2018. Cosmology and Dark Matter. *arXiv preprint arXiv:1802.02414*.

Townsend, P. K., 1997. Black holes. *arXiv preprint gr-qc/9707012*.

Tully, R. B. & Fisher, J. R., 1977. A new method of determining distances to galaxies. *Astronomy and Astrophysics*, **54**, 661–673.

Vikhlinin, A., Kravtsov, A., Forman, W., Jones, C., Markevitch, M., Murray, S. & Van Speybroeck, L., 2006. Chandra sample of nearby relaxed galaxy clusters: Mass, gas fraction, and mass-temperature relation. *The Astrophysical Journal*, **640**(2), 691.

Will, C. M., 2018. *Theory and experiment in gravitational physics*. Cambridge university press.

Williams, T. & Kelley, C., 2020. URL `http://www.gnuplot.info/`.

Zwicky, F., 1933. The redshift of extragalactic nebulae. *Helv. Phys. Acta*, **6**(110), 138.